Biosensors and Bioelectronics 87 (2017) 802–806

Contents lists available at ScienceDirect

Biosensors and Bioelectronics

journal homepage: www.elsevier.com/locate/bios

An ultrasensitive electrochemiluminescence biosensor for the detection of concanavalin A based on Au nanoparticles-thiosemicarbazide functionalized PtNi nanocubes as signal enhancer

Yu Fan[a], Xingrong Tan[b], Xin Ou[a], Shihong Chen[a,*], Shaping Wei[a,*]

[a] Key Laboratory of Luminescent and Real-Time Analytical Chemistry (Southwest University), Ministry of Education, College of Chemistry and Chemical Engineering, Southwest University, Chongqing 400715, China
[b] Department of Endocrinology, 9th People's Hospital of Chongqing, Chongqing 400700, China

ARTICLE INFO

Keywords:
Electrochemiluminescence
PtNi nanocube
ConA
Peroxydisulfate/oxygen system

ABSTRACT

A sandwich-configuration electrochemiluminescence (ECL) biosensor was constructed for detecting concanavalin A (ConA) based on peroxydisulfate/oxygen $\left(S_2O_8^{2-}/O_2\right)$ system. In this work, the gold nanoflower modified Zn-doped SnO_2 was used as a substrate to adsorb recognition element horseradish peroxidase (HRP) for binding ConA. Then, Au nanoparticles-thiosemicarbazide functionalized PtNi nanocubes (AuNPs-TSC-PtNi NCs), as a novel ECL signal tracer, were incubated onto the electrode through a specific carbohydrate-ConA interaction, thus achieving a sandwiched structure. The integration of amplifying effect of both TSC and PtNi NCs on the ECL of $S_2O_8^{2-}/O_2$ system endowed the biosensor a high sensitivity. The linear range for ConA detection was from 0.0010 ng/mL to 10 ng/mL with a detection limit of 0.0002 ng/mL (S/N=3).

1. Introduction

Noble metallic nanocrystals have drawn wide attention for many decades due to their high specific surface area, superior biocompatibility, excellent optical performances and outstanding electronic properties (Tian et al., 2007; Hong et al., 2012). Recently, a series of binary Pt-based alloys with several transition metals have frequently been used to improve the catalytic activity for the redox of H_2O_2 compared to the corresponding monometallic systems (Schrinner et al., 2009; Lu et al., 2008). Furthermore, the catalytic properties of platinum nanostructures are strongly dependent on their morphology and composition (Tian et al., 2007; Xu et al., 2014). In general, the faceted nanoparticles exhibited a higher catalytic activity as compared to spherical particles (Ren and Tilley, 2007; Han et al., 2008). Among various high-index facets (HIFs) nanocrystals, cubic Pt-based nanoparticles have drawn much attention owing to their unique structure and surface properties, as well as excellent electrocatalytic activities (Chou et al., 2012; Khi et al., 2015). Especially, PtNi nanocubes (PtNi NCs), with high specific surface area and good biocompatibility, could act as an outstanding nanocarrier. And also PtNi NCs demonstrated a good stability in the electrooxidation of both methanol and formic acid (Xu et al., 2014).

Electrochemiluminescence (ECL) techniques have witnessed a significant progress in the bisensing field due to the merits of low cost, easy operation, and high detection sensitivity (Wu et al., 2013; Dong et al., 2014). The inherent virtues of PtNi NCs drive the dreams of exploring their possible applications in ECL. However, Pt-based nanocubes were generally fabricated through a complicated process using electrochemistry (Peng et al., 2010), aqueous (Zhao et al., 2002) or non-aqueous synthetic routes (Lim et al., 2010). In this work, a one-pot wet-chemical reduction route was proposed for synthesizing PtNi NCs using polyvinylpyrrolidone (PVP), glycine, $NiCl_2$, and H_2PtCl_6. And so far, the application of PtNi NCs in ECL platform is still scarce.

Since Koval'chuk et al. reported the ECL behavior of peroxydisulfate ($S_2O_8^{2-}$) solution (Reshetnyak and Koval'chuk, 1998), the $S_2O_8^{2-}$/oxygen ($S_2O_8^{2-}/O_2$) system itself attracted increasing interest in ECL biosensor construction due to its merits of cheapness and accessibility (Yao et al., 2008). The ECL mechanisms of $S_2O_8^{2-}/O_2$ system are follows (Yao et al., 2008):

$$S_2O_8^{2-} + e \rightarrow SO_4^{\bullet-} + SO_4^{2-}SO_4^{\bullet-} + H_2O \rightarrow HO^{\bullet} + HSO_4^-HO^{\bullet}$$
$$\rightarrow HOO^{\bullet} + H_2OO_2 + H_2O + e \rightarrow HOO^{\bullet} + HO^-SO_4^{\bullet-} + HOO^{\bullet}$$
$$\rightarrow HSO_4^- + {}^1\left(O_2\right)_2{}^*{}^1\left(O_2\right)_2{}^* \rightarrow 2^3O_2 + h\nu$$

Above mechanisms indicated that the concentration of the dissolved oxygen had direct influence on the ECL signal, so increasing the concentration of the dissolved oxygen would be an effective way to enhance the sensitivity of $S_2O_8^{2-}/O_2$ system (Wang et al., 2014). When

* Corresponding authors.
E-mail addresses: cshong@swu.edu.cn (S. Chen), shapingw@swu.edu.cn (S. Wei).

http://dx.doi.org/10.1016/j.bios.2016.09.015
Received 9 July 2016; Received in revised form 24 August 2016; Accepted 4 September 2016
Available online 05 September 2016
0956-5663/

proper amounts of H_2O_2 existed in the detection solution, PtNi NCs exhibited excellent catalytic activity toward H_2O_2 to in situ generate O_2 around the electrode surface, thus amplifying the ECL signal.

The interactions between carbohydrates and specific lectins proteins mediated many important physiological and patho-physiological processes including bacterial and viral infections, cancer metastasis, inflammation, and immune surveillance (Lis and Sharon, 1998; Sharon and Lis, 1989). Therefore, the study of the interactions between carbohydrates and specific lectins proteins is very important for understanding important biological processes and for developing biosensors (Tang et al., 2013). Especially, concanavalin A (ConA), one of the most commonly studied lectins extracted from the jack bean, exists as a dimmer below pH 5.5 and a tetramer between pH 5.8 and pH 7.0 (molecular mass, 104,000 for tetramer) (Cella et al., 2010). And it has an affinity for mannose, glucose and some glycoproteins, such as horseradish peroxidase (HRP) and glucose oxidase (GOD) (Mallardi et al., 2015). At present, various methods have been reported to detect ConA, such as electrochemical methods (Liu et al., 2014), surface plasmon resonance (Huang et al., 2013) and fluorescence measurement (Zou et al., 2008). The reports concerning the detection of ConA with $S_2O_8^{2-}/O_2$ ECL system are relatively scarce now.

Recently, many researches focused on the development of bifunctional oxide materials due to their high chemical stability, low cost, nontoxicity and excellent electro-optical properties (Weng et al., 2015; Guan et al., 2014). Among these materials, Zn-doped SnO_2, with unique optical, catalytic, and electrical properties, has drawn considerable attention in lithium-ion batteries, solar cells and photocatalysts (Katoch et al., 2016; Dou et al., 2011). Moreover, the large specific surface area makes it could act as a good matrix to explore a novel immobilization and biosensing platform.

In this work, the nanocomposites of Zn-doped SnO_2 and gold nanoflower (AuNF/Zn-SnO_2) were used as matrix for high loading of horseradish peroxidase (HRP), which served as the recognition element for binding ConA. Thiosemicarbazide-Au nanoparticles functionalized PtNi nanocubes (AuNPs-TSC-PtNi NCs), as novel electrochemiluminescence (ECL) signal tracer, were synthesized and used to adsorb glucose oxidase (GOD), which could bind the ConA through a specific carbohydrate-ConA interaction. In this strategy, TSC could not only offer the active groups $-NH_2$ and $-SH$ to absorb AuNPs and PtNi NCs but also remarkably enhance the ECL signal of the $S_2O_8^{2-}/O_2$ system (Ma et al., 2015). During the fabrication of the biosensor, HRP, ConA and GOD-AuNPs-TSC-PtNi NCs formed a sandwiched structure. When the appropriate amount of D-glucose was added in the detection solution, GOD catalyzed the oxidization of D-glucose to produce gluconic acid accompanied by the generation of H_2O_2, which was further catalyzed by the PtNi NCs for the in-situ generation of O_2 for ECL signal amplification. The details of the preparation, characterization, optimization of conditions and the response performances of the biosensor are followings.

2. Experimental

2.1. Reagents and chemicals

$K_2S_2O_8$ and glucose were purchased from Chengdu Chemical Reagent Co. (Chengdu, China). Ascorbic acid (AA) was purchased from Chemical Reagent Co. (Chongqing, China). Glucose oxidase (GOD), horseradish peroxidase (HRP), bovine serum albumin (BSA, 96–99%), concanavalin A (ConA, from jack bean), phytohaemagglutinin and $SnCl_4{\cdot}5H_2O$ were purchased from Sigma Chemical Co. (St. Louis, MO, USA). Glycine and $HAuCl_4{\cdot}4H_2O$ were purchased from Kangda Amino Acid Company (Shanghai, China). AuNPs were synthesized chemically according to the method descibed by Frens (Frens, 1973). 3-aminopropyltrimethoxysilane (APTES), poly(vinyl pyrrolidone) (PVP, MW=30000), thiosemicarbazide (TSC), NaOH, $NiCl_2{\cdot}6H_2O$, $H_2PtCl_6{\cdot}6H_2O$, and $Zn(Ac)_2{\cdot}2H_2O$ were bought from Sinopharm Chemical Reagent Co. Ltd. (China). Phosphate buffered saline (PBS) solutions (0.10 M) with various pH were prepared using 0.10 M K_2HPO_4 and 0.10 M KH_2PO_4. The supporting electrolyte was 0.10 M KCl. Deionized water was used throughout this study.

2.2. Apparatus

The ECL emission was measured with a model MPI-E electrochemiluminescence analyzer (Xi'an Remax Electronic Science & Technology Co. Ltd. Xi'an, China) and the voltage of the photomultiplier tube (PMT) was set at 800 V and the potential scan is from 0 to −2.0 V during the detection. Cyclic voltammetry (CV) and electrochemical impedance spectroscopy (EIS) measurements were carried out with a CHI 600D electrochemical work station (Shanghai CH Instruments, China). A common three electrode system was used with a modified glassy carbon electrode (GCE, Φ=4.0 mm) as working electrode, a platinum wire as the auxiliary and a saturated calomel electrode (SCE) as the reference electrode for electrochemical experiments, or Ag/AgCl as the reference electrode for ECL experiments. Scanning electron microscopy (SEM) was carried out on the S-4800 (Hitachi Instruments Co., Japan). Energy-dispersive X-ray spectroscopy (EDS) was measured by SEM (SU8010, Hitachi, Japan). X-ray photoelectron spectroscopy (XPS) was test on Thermo ESCALAB 250 spectrometer (SID-Molecular).

2.3. Preparation of PtNi NCs

The PtNi NCs were prepared following the previously reported literature (Xu et al., 2014) with a slight modification. PVP (220 mg), glycine (58 mg), $NiCl_2$ aqueous solution (1.66 mM, 4 mL), and H_2PtCl_6 aqueous solution (20 mM, 1 mL) were mixed and stirred for 5 min, and then sonicated for 5 min at room temperature. The resulting homogeneous yellow solution was sealed in a 20 mL Teflon-lined autoclave and maintained at 200 °C for 6 h. After cooling to room temperature, the PtNi NCs were separated by centrifugation at 9200 rpm for 15 min and washed several times with ethanol.

2.4. Preparation of GOD-AuNPs-TSC-PtNi NCs

The preparation process of GOD-AuNPs-TSC-PtNi NCs was shown in Scheme 1A. Briefly, 300 μL 20 mM TSC was added into PtNi NCs solution with stirring, followed by centrifugation and washing twice with deionized water, and dispersed in 1 mL PBS (pH 7.4). Then 300 μL of the prepared AuNPs solution was added into the mixture for about 12 h with stirring. The AuNPs-TSC-PtNi NCs nanocomposites were obtained by centrifugation at 9000 rpm for 15 min at 4 °C to discard excess reagents, and redispersed in 1 mL PBS (pH 7.4). Subsequently, 1 mL of GOD (1 mg/mL) was added into the dispersion of AuNPs-TSC-PtNi NCs under gentle stirring for about 4 h at 4 °C. The precipitate was collected by centrifugation and dispersed in deionized water. Then 50 μL of BSA (0.25%) was ultimately added to the mixture for about 1 h to block the non-specific adsorption. At last, the GOD-AuNPs-TSC-PtNi NCs was collected by centrifugation and redispersed in 1 mL PBS (pH 7.4) and then stored at 4 °C when not used. For comparison, GOD-AuNPs and GOD-AuNPs-TSC were prepared using a similar method.

2.5. Preparation of AuNF/Zn-SnO_2

Firstly, Zn-SnO_2 was prepared by a simple one-step hydrothermal method (Dou et al., 2011). Initially, 0.02 mM $Zn(Ac)_2$, 1.0 mM $SnCl_4$ and 15.0 mM NaOH were successively introduced into a 30 mL mixture solution of ethanol and deionized water. Next, the mixture was transferred into a 50 mL Teflon-lined autoclave and maintained at 180 °C for 24 h. When cooled to room temperature, the Zn-SnO_2 was gathered by centrifugation and washed.

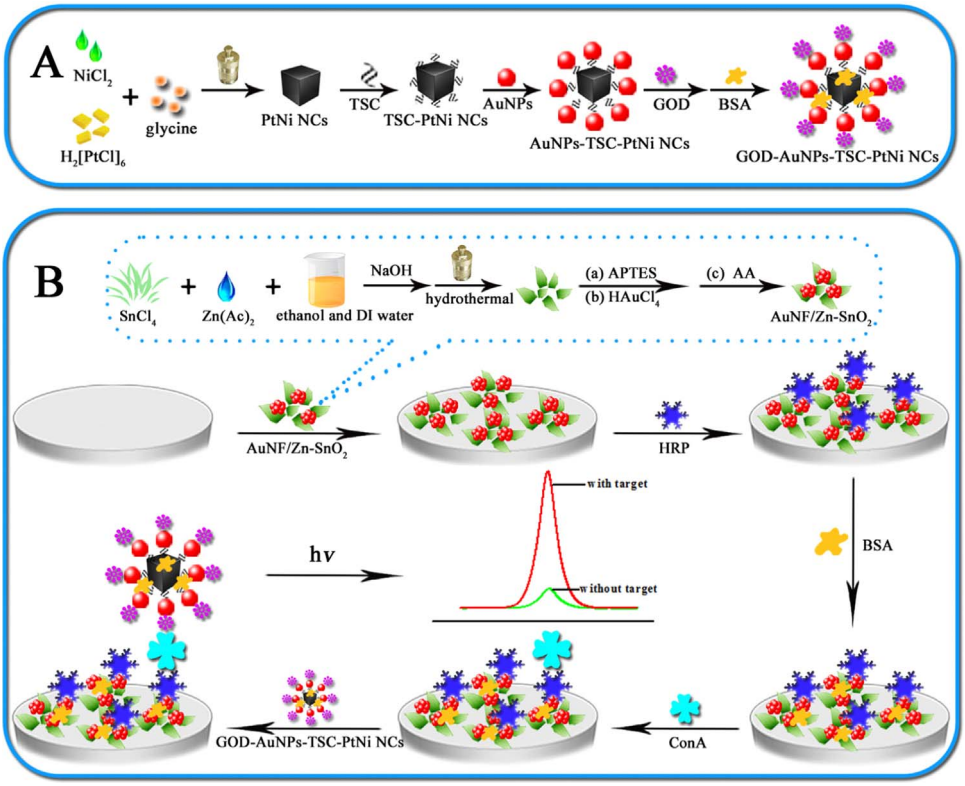

Scheme 1. The illustration of the synthetic process of (A) GOD-AuNPs-TSC-PtNi NCs and (B) the preparation of the ECL biosensor.

Secondly, the AuNF/Zn-SnO_2 hybrids were synthesized as follows. 30 μL APTES was added into the Zn-SnO_2 dispersion. The mixture was stirred at room temperature overnight. Then, amino-functionalized Zn-SnO_2 was obtained by centrifugation, and washed for three times with absolute ethanol, and redispersed in 2 mL deionized water for further use. 50 μL of 1% $HAuCl_4$ solution was added into above amino-functionalized Zn-SnO_2 suspension with stirring for 1 h, and then left undisturbed for 10 h to allow the adsorption of $AuCl_4^-$ on Zn-SnO_2 to form a seed solution. Then, 100 μL of 1.0% $HAuCl_4$ solution was added into the seed solution under stirring. After that, AA was added into the mixture in situ to form AuNF on the Zn-SnO_2. Followed by centrifugation, the AuNF/Zn-SnO_2 was obtained and stored at 4 °C until use.

2.6. Fabrication of the ECL biosensor

A glassy carbon electrode (GCE, Φ=4.0 mm) was first polished with 0.3 and 0.05 μm alumina powder, followed by successive sonication in ethanol and deionized water. After that, 10 μL of AuNF/Zn-SnO_2 dispersion was dropped onto the pretreated GCE and then dried in the air. Subsequently, 10 μL of HRP solution (2 mg/mL) was incubated on the electrode for 8 h. Then, 10 μL of BSA (0.2 wt%) was dropped onto the surface of modified electrode to eliminate the nonspecific binding effects. During the fabrication of the biosensor, for each modification step, the electrode was washed with PBS to eliminate the nonspecific binding. The fabrication of the biosensor is shown in Scheme 1B and the obtained biosensor (BSA/HRP/AuNF/Zn-SnO_2/GCE) was stored at 4 °C for further use.

2.7. Measurement procedure

The prepared biosensor was incubated with various concentrations of ConA (10 μL) for 1 h. In this step, ConA would be captured by HRP through specific binding between ConA and sugar residues of the enzymes (Mallardi et al., 2015). The modified electrode was further incubated with 10 μL GOD-AuNPs-TSC-PtNi NCs through a similar carbohydrate-ConA interaction for 1 h to achieve the sandwich configuration. The obtained biosensor was measured with a MPI-E ECL analyzer in 0.10 M pH 7.0 PBS containing 0.10 M $K_2S_2O_8$ and 0.030 M glucose at room temperature.

3. Results and discussion

3.1. Characterization of different nanomaterials

Microstructures and morphologies of the different nanomaterials were characterized by SEM. As can be seen in the SEM image of PtNi NCs (Fig. 1A), a cube-like shape with uniform particle size and shape distribution can be observed. And also the stereostructure of the PtNi NCs can be clearly observed, indicating the successful synthesis of PtNi NCs. XPS measurements were further performed to gain the information concerning the chemical composition of PtNi NCs. As seen in Fig. 1B, the most intense doublet with binding energies of 70.38 eV (Pt $4f_{7/2}$) and 73.68 eV (Pt $4f_{5/2}$) was attributed to metallic Pt (Gao et al., 2011). The negative shift as compared to pure metallic Pt ($4f_{7/2}$: 70.90 eV) was probably due to the electron donating from Ni to Pt (Xu et al., 2014). In particular, the peak intensity of Ni 2p was quite weak (Fig. 1C).

As shown in Fig. 1D, the melon seeds-like of Zn-SnO_2 was clearly observed. For the SEM image of AuNF/Zn-SnO_2 hybrids (Fig. 1E), the bright spherical gold nanoparticles were observed on the surface of Zn-SnO_2, indicating the successful synthesis of AuNF/Zn-SnO_2 hybrids. The EDS spectrum (Fig. 1F) of the AuNF/Zn-SnO_2 clearly showed the existence of Sn, Zn, Au and O elements, also revealing the successful synthesis of AuNF/Zn-SnO_2 hybrids.

3.2. ECL and CV characterization of stepwise fabrication of the electrode

Scheme 1B pictures the stepwise assembly of the biosensor, which was characterized using ECL and CV. ECL measurement was per-

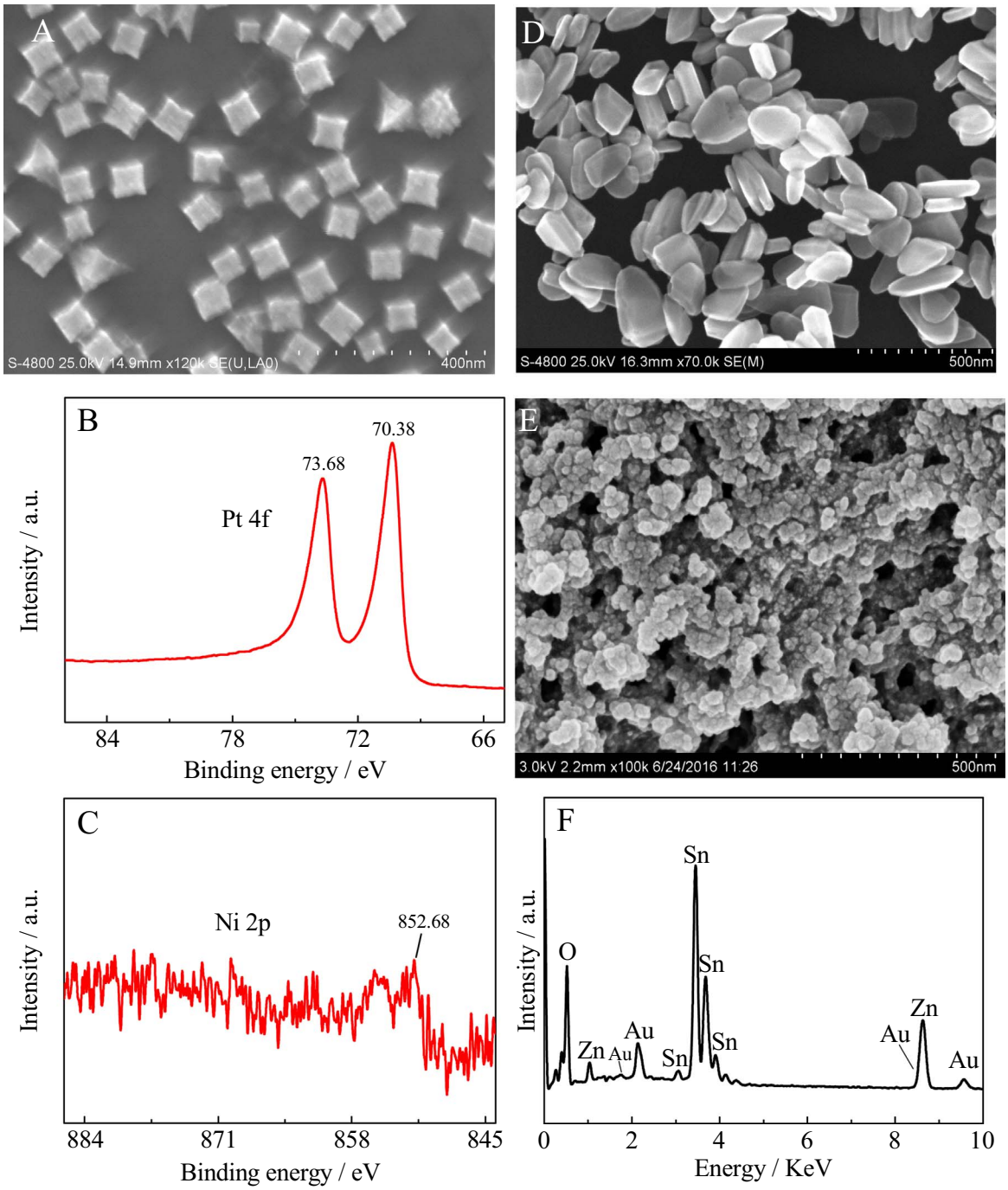

Fig. 1. SEM images of (A) PtNi NCs, (D) Zn-SnO_2, and (E) AuNF/Zn-SnO_2. The XPS patterns of (B) Pt 4f and (C) Ni 2p. (F) EDS spectra of Zn-SnO_2.

formed in 3 mL PBS (pH 7) containing 0.10 M $K_2S_2O_8$. As indicated by the ECL dynamic curve (Fig. 2A) and ECL potential curve (Fig. 2A inset), relative low ECL intensity appeared at the bare GCE (curve a). When AuNF/Zn-SnO_2 was cast on the GCE, an increase in ECL intensity was observed (curve b) due to the fact that AuNF could promote the electrochemical reaction efficiency of $S_2O_8^{2-}/O_2$ system. When HRP, BSA and ConA were successively modified onto the electrode (curves c–e), continuous decreased ECL intensity was observed because of the obstacle of these non-conductive materials. Additionally, as shown in Fig. 1A inset, ECL peak appeared at approximate −2.0 V, which was the luminous potential from the light emitting specie $^1(O_2)_2$ (Yao et al., 2008).

The electrochemical characterization of the stepwise-modified electrode was obtained by CV in 5.0 mM $K_3[Fe(CN)_6]/K_4[Fe(CN)_6]$ and the results are shown in Fig. 2B. As seen, a couple of quasi-reversible redox peaks of the probes was noticed at the bare electrode (curve a). When the electrode was modified with AuNF/Zn-SnO_2, an increase in the peak current was observed (curve b). This was due to the fact that AuNF/Zn-SnO_2 could accelerate the electron transfer between the $Fe(CN)_6^{4-/3-}$ and the electrode. When HRP, BSA and ConA were successively modified onto the electrode (curves c–e), the redox peak currents continuously decreased due to the insulation of HRP, BSA and ConA. The ECL and CV studies proved that the biosensor has been successfully prepared.

3.3. Optimization of experimental conditions

As is well known, the pH is important for the performance of the biosensor. Hence, the influence of pH on the ECL behavior of the

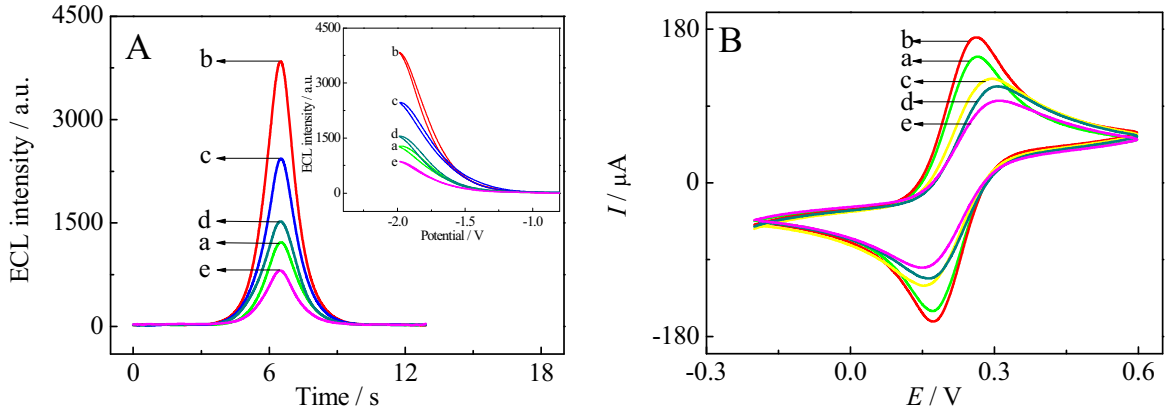

Fig. 2. (A) ECL responses in 0.10 M PBS (pH 7) containing 0.10 M $K_2S_2O_8$ and (B) CV curves in 5.0 mM $K_3[Fe(CN)_6]/K_4[Fe(CN)_6]$ at (a) bare GCE, (b) AuNF/Zn-SnO_2/GCE, (c) HRP/AuNF/Zn-SnO_2/GCE, (d) BSA/HRP/AuNF/Zn-SnO_2/GCE, and (e) ConA/BSA/HRP/AuNF/Zn-SnO_2/GCE. Scan rate: 100 mV/s for ECL measurements, 50 mV/s for CV measurements.

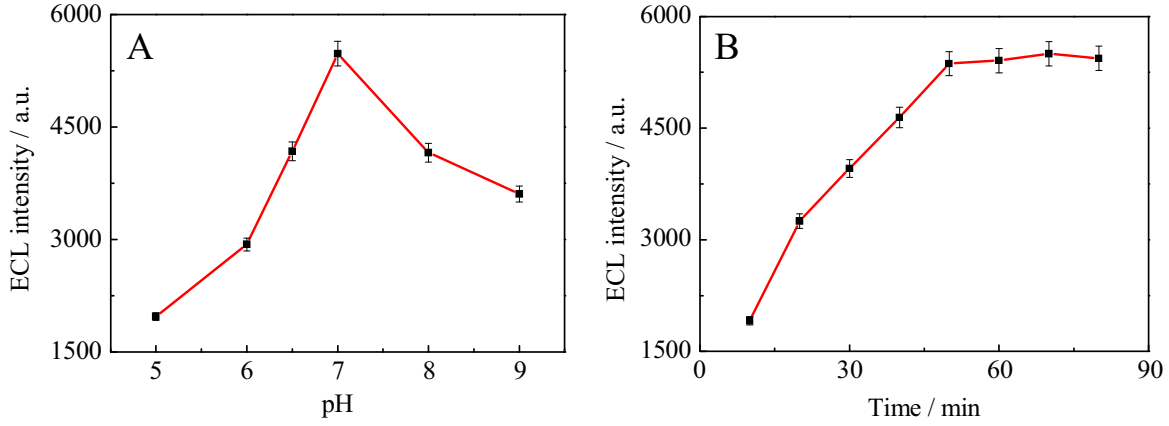

Fig. 3. Effect of (A) pH of PBS and (B) the incubation time of ConA on the ECL response of the biosensor to 0.10 ng/mL ConA in PBS (pH 7) containing 0.10 M $K_2S_2O_8$. Scan rate: 300 mV/s. Scan voltage: −2.0–0.0 V.

working electrode was studied. As shown in Fig. 3A, the ECL intensity increased when pH varied from 5.0 to 7.0, then fell down as pH ranged from 7.0 to 9.0. So, pH 7.0 was chosen as the optimal pH.

The effect of the incubation time of ConA on the ECL intensity was also investigated. As seen from Fig. 3B, the ECL intensity increased with the increase in the incubation time from 10 to 50 min and then remained relatively stable after 50 min. So the incubation time of 50 min was selected as the optimal time.

3.4. ECL behaviors of different modified electrodes

The effect of AuNF and Zn-SnO_2 on the ECL signal of $S_2O_8^{2-}/O_2$ system was investigated and the results are shown in Fig. 4A. As seen from Fig. 4A, compared with the bare electrode (curve a), a slight increase in ECL signal was observed at the Zn-SnO_2/GCE (curve b). With the introduction of AuNF, an obvious increase in ECL intensity was observed at the AuNF/Zn-SnO_2 modified electrode (curve c). Thus, in this work, AuNF/Zn-SnO_2 was chosen as the substrate to adsorb recognition element horseradish peroxidase (HRP). Although Zn-SnO_2 didn't significantly enhance the ECL signal of $S_2O_8^{2-}/O_2$ system, more importantly, Zn-SnO_2 served as the supporter for the in situ synthesis of AuNF. The good membrane-forming property and large specific surface area of Zn-SnO_2 were favorable to the in situ growth of AuNF, thus achieving the high loading of recognition element HRP on the AuNF/Zn-SnO_2 for binding ConA.

To confirm the amplifying effect of TSC and PtNi NCs in $S_2O_8^{2-}/O_2$ ECL system, different conjugates were prepared including BSA-GOD-AuNPs, BSA-GOD-AuNPs-TSC and BSA-GOD-AuNPs-TSC-PtNi NCs. The changes of ECL intensity at the biosensor (BSA/HRP/AuNF/Zn-SnO_2/GCE) modified with different conjugates are shown in the Fig. 4B/C/D. For the biosensor incubated with the BSA-GOD-AuNPs conjugate, the ECL signal increased about 788.6 a.u. (Fig. 4B). Such an increase might be ascribed to the fact that AuNPs had outstanding eletroconductivity, which accelerated the electron transfer between $S_2O_8^{2-}$ and the electron surface to obtain more luminescent intermediate $SO_4^{\bullet-}$ at the unit time (Zhuo et al., 2014). For the biosensor incubated with the BSA-GOD-AuNPs-TSC conjugate, the ECL emission increased about 2587 a.u. (Fig. 4C), which was greater than that in the case of BSA-GOD-AuNPs (Fig. 4B). This is because that TSC could act as the co-reactant to increase the ECL response of the $S_2O_8^{2-}/O_2$ system (Ma et al., 2015). The possible mechanism of the signal amplification strategy was as follows:

$$S_2O_8^{2-} + e \rightarrow SO_4^{\bullet-} + SO_4^{2-} \quad (1)$$

$$SO_4^{\bullet-} + H_2O \rightarrow HO^{\bullet} + HSO_4^{-} \quad (2)$$

$$HO^{\cdot} \rightarrow HOO^{\cdot} + H_2O \quad (3)$$

$$TSC - e \rightarrow TSC^{\cdot+} \quad (4)$$

$$TSC^{\cdot+} \rightarrow TSC^{\cdot} + H^{+} \quad (5)$$

$$HOO^{\cdot} + TSC^{\cdot} \rightarrow TSC + {}^1(O_2)_2{}^* \quad (6)$$

$${}^1(O_2)_2{}^* \rightarrow 2\,{}^3O_2 + h\nu \quad (7)$$

As expected, the prepared BSA-GOD-AuNPs-TSC-PtNi NCs conjugates (Fig. 4D) exhibited a much higher ECL signal than others two

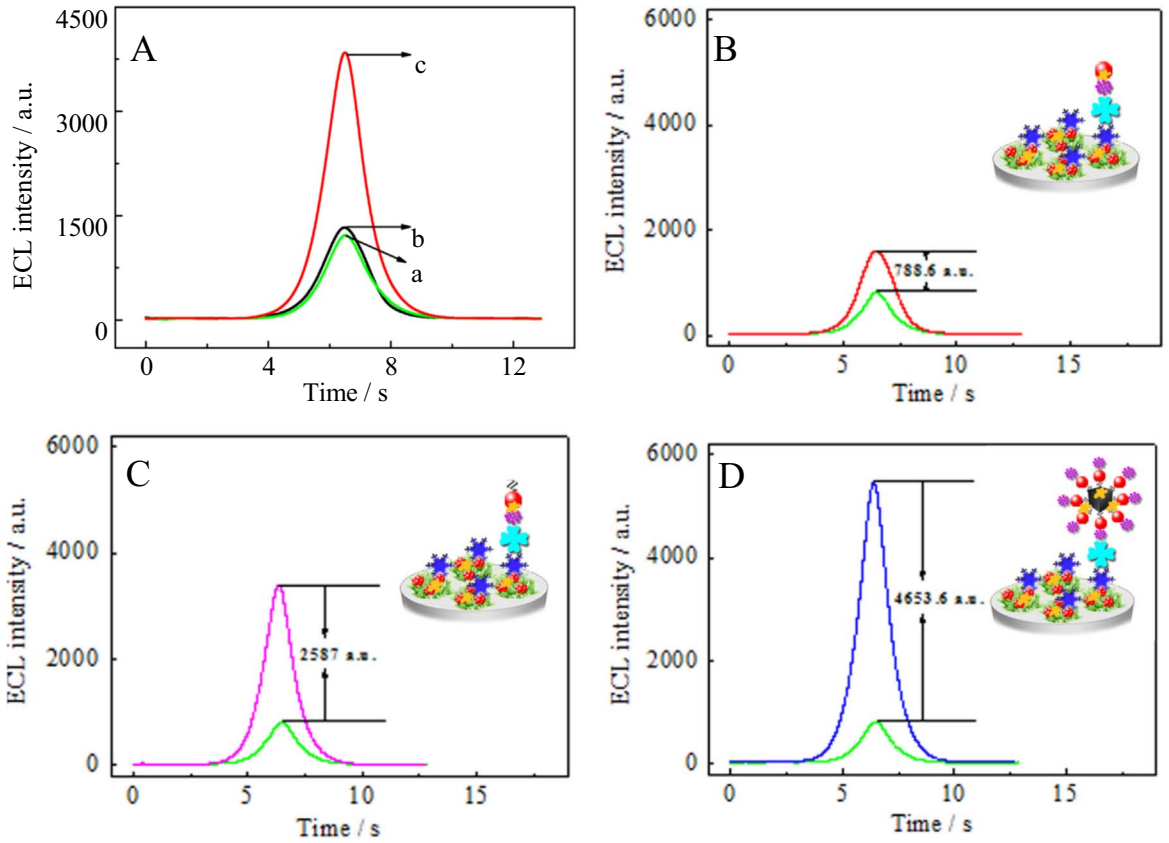

Fig. 4. (A) ECL responses in 0.10 M PBS (pH 7) containing 0.10 M $K_2S_2O_8$ at (a) bare GCE, (b) Zn-SnO_2/GCE, and (c) AuNF/Zn-SnO_2/GCE. The comparison of ECL responses at the biosensor with different conjugates: (B) BSA-GOD-AuNPs, (C) BSA-GOD-AuNPs-TSC, and (D) BSA-GOD-AuNPs-TSC-PtNi NCs in the case of 0.10 ng/mL ConA incubated on the biosensor.

cases. The reasons are generalized as follows. (1) Both TSC and AuNPs could enhance the ECL response of $S_2O_8^{2-}/O_2$ system. (2) When the appropriate amount of D-glucose was added into the detection solution, GOD catalyzed the oxidization of D-glucose to produce gluconic acid accompanied by the generation of H_2O_2, which was further catalyzed by the PtNi NCs to in-situ generate O_2 for the ECL signal amplification. The electrocatalytic behavior of PtNi NCs toward H_2O_2 was shown in the supplementary and Fig. S1. (3) PtNi NCs exhibited a large specific surface area, which could act as a good carrier for high loading of BSA-GOD-AuNPs-TSC. Thus, the BSA-GOD-AuNPs-TSC-PtNi NCs conjugate was adopted for the sandwich-type biosensor to obtain much greater signal amplification and higher detection sensitivity.

3.5. Performance of the biosensor

Under the optimized experimental conditions, the quantitative range of the prepared ECL biosensor for the detection of ConA was explored. As shown in Fig. 5, ECL signal enhanced gradually with increasing the concentration of ConA. The relationship between ECL intensity and the logarithm of concentrations of ConA is illustrated in the insert of Fig. 5. As seen, the ECL intensity exhibited a good linear relationship with the target ConA concentration in the range from 0.0010 ng/mL to 10 ng/mL. The linear regression equations were obtained as I=20363.3+1483.7 log$c$ (R=0.999), and the detection limit was calculated to be 0.0002 ng/mL (S/N=3). Here, I represents the ECL intensity and c stands for the concentration of ConA. The analytical performance of our proposed ECL biosensor was compared with others previous reports and the results are shown in Table 1. Obviously, our prepared biosensor exhibited a lower detection limit and a wider linear range. The reason is as follows. Every nanomaterial used in this strategy played an important role to improve the

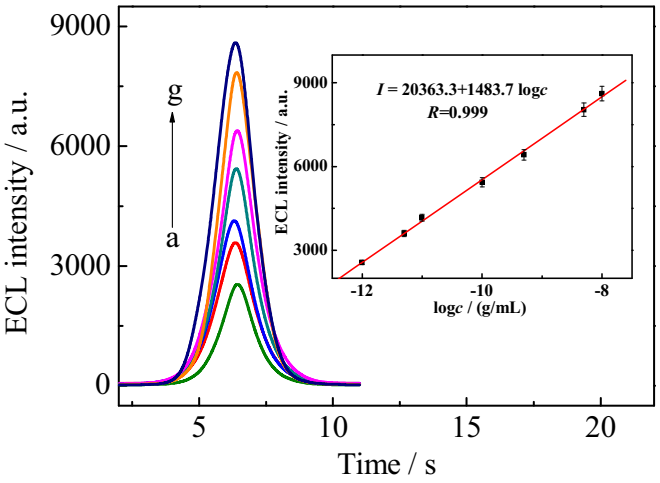

Fig. 5. ECL responses of the biosensor to (a) 0.0010, (b) 0.0050, (c) 0.010, (d) 0.10, (e) 0.50, (f) 5.0 and (g) 10 ng/mL ConA in PBS (pH 7) containing 0.10 M $K_2S_2O_8$. Scan rate: 300 mV/s. Scan voltage: −2.0–0.0 V. Inset showed the linear calibration curve.

sensitivity. Firstly, the good membrane-forming property and large specific surface area of Zn-SnO_2 were favorable to the in situ growth of AuNF, thus achieving the high loading of recognition element horseradish peroxidase (HRP) on the AuNF/Zn-SnO_2 for binding more targets ConA. Secondly, PtNi NCs, AuNPs and TSC can remarkably enhance the ECL signal of $S_2O_8^{2-}/O_2$ system. Thirdly, the ECL technique itself has high sensitivity. Based on the combination of above advantages, signal-on assays with a high sensitivity is easy to achieve.

Table 1
Comparison of different methods for the determination of ConA.

Method	Linear range (μg/mL)	Detection limit (μg/mL)	Reference
Differential pulse voltammetry	3.4×10^{-4}–9.5×10^{-1}	1.1×10^{-4}	Hu et al., 2012
Electrochemiluminescence	5.0×10^{-5}–1.0×10^{-1}	1.7×10^{-5}	Ou et al., 2015
Electrochemistry			

3.6. Selectivity and stability of the biosensor

Some interfering agents including BSA, cytochrome c (Cyt C), and phytohemagglutinin (PHA), were applied to explore the selectivity of the prepared biosensor. As depicted in Fig. S2A, the ECL intensity of the biosensor incubated with BSA, Cyt C or PHA was similar to that of the blank sample. Meanwhile, an obviously enhanced ECL response was obtained after incubation with ConA. And no obvious changes in ECL intensity were observed when comparing the response of the mixture of ConA and different interfering agents to that in the case of alone ConA. Above results indicated a good selectivity of the biosensor.

Stability is of great importance to judge the performance of the biosensor. In order to explore whether the biosensor could meet the needs of continuous cyclic scans for long testing process, the stability of the prepared biosensor was studied under continuous scanning for 12 cycles. As seen in Fig. S2B, the ECL response did not show any significant changes and the relative standard deviation (RSD) was 1.1%. The experimental result indicated that the proposed biosensor had good stability.

3.7. Application of the biosensor

The practical applicability of the designed biosensor was studied by detecting ConA in human serum samples using a standard addition method. From results in Table S1, the recoveries were ranging from 95% to 106%, demonstrating the practicability of designed biosensor for ConA detection in real biological samples.

4. Conclusions

In this work, a novel and ultrasensitive ECL detection method for ConA was constructed using AuNPs-TSC-PtNi NCs as ECL signal tracer in $S_2O_8^{2-}/O_2$ system. TSC could not only offer the active groups $-NH_2$ and $-SH$ to absorb AuNPs and PtNi NCs but also remarkably enhance the ECL signal of $S_2O_8^{2-}/O_2$ system. PtNi NCs could not only act as a good carrier for high loading of GOD-AuNPs-TSC, but also could amplify the ECL signals. The constructed biosensor exhibited excellent sensitivity, selectivity and reproducibility, holding a promise in the detection of ConA. Moreover, the employment of the novel ECL signal tracer AuNPs-TSC-PtNi NCs in $S_2O_8^{2-}/O_2$ system would open a new ECL platform.

Acknowledgments

This work was supported by the National Natural Science Foundation of China (51473136, 21575116), the Natural Science Foundation Project of Chongqing City (CSTC-2014JCYJA20005) and the Fundamental Research Funds for the Central Universities (XDJK2015A002, SWU115004), China.

Appendix A. Supplementary material

Supplementary data associated with this article can be found in the online version at http://dx.doi.org/10.1016/j.bios.2016.09.015.

References

Cella, L.N., Chen, W., Myung, N.V., Mulchandani, A., 2010. J. Am. Chem. Soc. 132, 5024–5026.
Chou, S.W., Shyue, J.J., Chien, C.H., Chen, C.C., Chen, Y.Y., Chou, P.T., 2012. Chem. Mater. 24, 2527–2533.
Dong, Y.Q., Tian, W.R., Ren, S.Y., Dai, R.P., Chi, Y.W., Chen, G.N., 2014. ACS Appl. Mater. Interfaces 6, 1646–1651.
Dou, X.C., Sabba, D., Mathews, N., Wong, L.H., Lam, Y.M., Mhaisalkar, S., 2011. Chem. Mater. 23, 3938–3945.
Frens, G., 1973. Nature 241, 20–22.
Gao, H.C., Xiao, F., Ching, C.B., Duan, H.W., 2011. ACS Appl. Mater. Interfaces 3, 3049–3057.
Guan, Y., Wang, D.W., Zhou, X., Sun, P., Wang, H.Y., Ma, J., Lu, G.Y., 2014. Sens. Actuators B: Chem. 191, 45–52.
Han, S.B., Song, Y.J., Lee, J.M., Kim, J.Y., Park, K.W., 2008. Electrochem. Commun. 10, 1044–1047.
Hong, J.W., Lee, S.U., Lee, Y.W., Han, S.W., 2012. J. Am. Chem. Soc. 134, 4565–4568.
Hu, F.X., Chen, S.H., Wang, C.Y., Yuan, R., Xiang, Y., Wang, C., 2012. Biosens. Bioelectron. 34, 202–207.
Huang, C.F., Yao, G.H., Liang, R.P., Qiu, J.D., 2013. Biosens. Bioelectron. 50, 305–310.
Katoch, A., Abideen, Z.U., Kim, H.W., Kim, S.S., 2016. ACS Appl. Mater. Interfaces 8, 2486–2494.
Khi, N.T., Park, J.S., Baik, H., Lee, H., Sohn, J.H., Lee, K., 2015. Nanoscale 7, 3941–3946.
Lim, S.I., Ojea-Jimenez, I., Varon, M., Casals, E., Arbiol, J., Puntes, V., 2010. Nano Lett. 10, 964–973.
Lis, H., Sharon, N., 1998. Chem. Rev. 98, 637–674.
Liu, B.Q., Zhang, B., Chen, G.N., Yang, H.H., Tang, D.P., 2014. Anal. Chem. 86, 7773–7781.
Lu, J., Do, I., Drzal, L.T., Worden, R.M., Lee, I., 2008. ACS Nano 2, 1825–1832.
Ma, M.N., Zhang, X., Zhuo, Y., Chai, Y.Q., Yuan, R., 2015. Nanoscale 7, 2085–2092.
Mallardi, A., Angarano, V., Magliulo, M., Torsi, L., Palazzo, G., 2015. Anal. Chem. 87, 11337–11344.
Ou, X., Tan, X.R., Liu, X.F., Lu, Q.Y., Chen, S.H., Wei, S.P., 2015. Biosens. Bioelectron. 70, 89–97.
Peng, Z.M., You, H.J., Wu, J.B., Yang, H., 2010. Nano Lett. 10, 1492–1496.
Ren, J., Tilley, R.D., 2007. J. Am. Chem. Soc. 129, 3287–3291.
Reshetnyak, O.V., Koval'chuk, E.P., 1998. Electrochim. Acta 43, 465–469.
Schrinner, M., Ballauff, M., Talmon, Y., Kauffmann, Y., Thun, J., Moller, M., Breu, J., 2009. Science 323, 617–620.
Sharon, N., Lis, H., 1989. Science 246, 227–234.
Tang, D.P., Zhang, B., Tang, J., Hou, L., Chen, G.N., 2013. Anal. Chem. 85, 6958–6966.
Tian, N., Zhou, Z.Y., Sun, S.G., Ding, Y., Wang, Z.L., 2007. Science 316, 732–735.
Wang, H.J., Bai, L.J., Chai, Y.Q., Yuan, R., 2014. Small 10, 1857–1865.
Weng, Y.Y., Zhang, L.C., Zhu, W., Lv, Y., 2015. J. Mater. Chem. A 3, 7132–7138.
Wu, M.S., Yuan, D.J., Xu, J.J., Chen, H.Y., 2013. Chem. Sci. 4, 1182–1188.
Xu, X.L., Zhang, X., Sun, H., Yang, Y., Dai, X.P., Gao, J.S., Li, X.Y., Zhang, P.F., Wang, H.H., Yu, N.F., Sun, S.G., 2014. Angew. Chem. Int. Ed. 53, 12522–12527.
Yan, S.G., Zhang, L.C., Tang, Y.R., Lv, Y., 2014. Analyst 139, 4210–4215.
Yao, W., Wang, L., Wang, H.Y., Zhang, X.L., 2008. Electrochim. Acta 54, 733–737.
Zhao, S.Y., Chen, S.H., Wang, S.Y., Li, D.G., Ma, H.Y., 2002. Langmuir 18, 3315–3318.
Zhuo, Y., Gui, G.F., Chai, Y.Q., Liao, N., Xiao, K., Yuan, R., 2014. Biosens. Bioelectron. 53, 459–464.
Zou, L., Pang, H.L., Chan, P.H., Huang, Z.S., Gu, L.Q., Wong, K.Y., 2008. Carbohydr. Res. 343, 2932–2938.